HHS Public Access

Author manuscript

Biomacromolecules. Author manuscript; available in PMC 2019 February 06.

Published in final edited form as:

Biomacromolecules. 2017 August 14; 18(8): 2419–2426. doi:10.1021/acs.biomac.7b00589.

Micellar self-assembly of perfectly sequence-defined recombinant resilin-like/elastin-like block copolypeptides

Isaac Weitzhandler[#a], **Michael Dzuricky**[#a], **Ingo Hoffmann**[b,§], **Felipe Garcia Quiroz**[a,†], **Michael Gradzielski**[b], and **Ashutosh Chilkoti**[a,*]

[a]Department of Biomedical Engineering and Research Triangle Materials Research Science and Engineering Center (RT-MRSEC), Duke University. Durham, NC 27708.

[b]Stranski-Laboratorium fur Physikalische und Theoretische Chemie, Institut für Chemie Technische Universität Berlin. 10623, Berlin, Germany

[#] These authors contributed equally to this work.

Abstract

This paper reports the synthesis of perfectly sequence defined, monodisperse diblock copolypeptides of a hydrophilic elastin-like polypeptide block and a hydrophobic resilin- like polypeptide block and characterization of their self-assembly as a function of structural parameters by light scattering, cryo-TEM, and small-angle neutron scattering. A subset of these diblock copolypeptides exhibit LCST and UCST phase behavior and self-assemble into spherical or cylindrical micelles. Their morphology is dictated by their chain length, degree of hydrophilicity and hydrophilic weight fraction of the ELP block. We find that: (1) independent of the length of the corona forming ELP block there is a minimum threshold in the length of the RLP block below which self-assembly does not occur, but that once that threshold is crossed, (2) the RLP block length is a unique molecular parameter to independently tune self-assembly; and (3) increasing the hydrophobicity of the corona-forming ELP drives a transition from spherical to cylindrical morphology. Unlike the self-assembly of purely ELP based block copolymers, the self-assembly of RLP-ELPs can be understood by simple principles of polymer physics relating hydrophilic weight fraction, polymer-polymer and polymer-solvent interactions to micellar morphology, which is important as it provides a route for the de novo design of desired nanoscale morphologies from first principles.

Graphical Abstract

[*]**Corresponding Author:** chilkoti@duke.edu.

[§]**Present Addresses** Institut Laue-Langevin. 71 avenue des Martyrs, 38000 Grenoble, France.

[†]The Rockefeller University. 1230 York Avenue, New York, NY 10065.

Author Contributions

The manuscript was written through contributions of all authors. All authors have given approval to the final version of the manuscript.

ASSOCIATED CONTENT

ELP sequences, turbidimetry plots, dynamic light scattering plots, plots of refractive index, static light scattering partial Zimm plots, additional cryo-TEM images, and SANS model details. This material is available free of charge at http://pubs.acs.org.

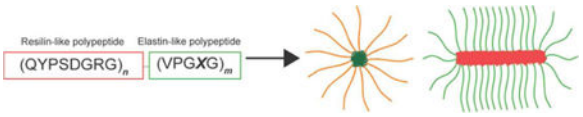

Keywords

Self-assembly; proteins; block copolymers; elastin-like polypeptides

1. Introduction

In recent decades, block copolymers —polymers composed of two or more distinct blocks— have been studied extensively. [1–2] When the blocks have a different solubility in a solvent of interest, block copolymers can self-assemble into a range of structures including micelles [3], vesicles (sometimes referred to as “polymersomes”) [4], and lamellae. [5] At the same time, polymers that display aqueous, temperature sensitive phase behavior, namely lower critical solution temperature (LCST) and the converse, upper critical solution temperature (UCST) transition have also been studied for decades. [6–7] With advances in polymer synthesis methodologies, these polymers have been combined to create diblock copolymers with an LCST and UCST exhibiting block. [8] Some of these synthetic LCST-UCST diblock copolymers exhibit dual LCST and UCST behavior that are capable of temperature triggered self-assembly [8], and a subset of these also exhibit micelle inversion in response to temperature, as the two blocks switch their hydrophobicity in response to an increase in solution temperature. [9–12]

Despite the significant body of work on synthetic LCST-UCST diblock copolymers, these studies have also revealed some significant lacunae. First, these diblock copolymers have shown limited morphologies upon self-assembly. Most extant studies report spherical morphologies [13–14], and few other morphologies such as vesicles [10], but in general, these observations are not backed by direct and unequivocal experimental conformation of the morphology of the putative self-assembled structures by scattering techniques or electron microscopy. Second, none of these studies have systematically explored structural parameters such as composition and weight fraction that critically impact the morphology of the self-assembled structures. Finally, none of these studies have elucidated the design rules that enable prediction of the morphologies of the self-assembled structures, even for systems with a narrowly defined composition. This paper addresses this important gap by the design of sequence controlled, monodisperse diblock copolymers of an LCST and UCST block and characterization of their self-assembled morphologies as a function of key structural parameters.

These studies were made possible by the fact that we recently identified a new set of recombinant peptide polymers that exhibit UCST behavior, that we have named resilin-like polypeptides (RLPs) [15], as they are inspired by the consensus sequence of native resilin. [16–18] The recent availability of a set of UCST exhibiting polypeptides that can be combined with well- studied elastin-like polypeptides (ELPs) that exhibit LCST behavior, provided for

the first time an opportunity for the systematic exploration of LCST-UCST diblock copolymers.

In this study, we systematically varied the length of the RLP block, which forms the core of the self-assembled micelles, to investigate the effect of hydrophilic weight fraction on self-assembly. We also independently varied the hydrophilicity of the corona-forming ELP block, to investigate the effect of corona chain hydrophilicity on self-assembly. Finally, we varied the overall length of the chains while keeping the hydrophilic weight fraction constant, to investigate the effect of molecular weight on self-assembly. To develop a complete picture of their self-assembly, we characterized the block copolypeptides by dynamic and static light scattering (DLS and SLS), cryogenic transmission electron microscopy (cryo-TEM), and small-angle neutron scattering (SANS).

We find that unlike most previously reported recombinant block copolypeptides [19–21], the presence or absence of nanoscale self-assembly and the morphology of the self-assembled constructs of resilin-like/elastin-like block copolypeptides are all predictably governed by simple principles of polymer physics. Specifically, their self-assembly is consistent with the relationship reported by Eisenberg and Discher that the balance between the hydrophilic and hydrophobic blocks (i.e. the hydrophilic weight fraction) determines the morphology, with a higher hydrophilic weight fraction leading to spherical micelles and a lower hydrophilic weight fraction leading to cylindrical micelles.[22–24]

2. Experimental section

2.1 Materials

Oligonucleotides encoding all polypeptide sequences were purchased from Integrated DNA Technologies (Coralville, IA). Competent E. coli EB5α cells, used for cloning, and BL21(DE3) cells, used for expression, were purchased from Edge BioSystems (Gaithersburg, MD). Terrific Broth (TB) Dry powder growth media was purchased from MO BIO Laboratories (Carlsbad, CA). Kanamycin sulfate was purchased from EMD Millipore (Billerica, MA) and isopropyl-beta-D-thiogalactoside (IPTG) was purchased from Gold Biotechnology (St. Louis, MO). Calbiochem phosphate buffered saline (PBS) tablets (10 mM phosphate buffer, 140 mM NaCl, 3 mM KCl, pH 7.4 at 25°C) were purchased from EMD Millipore (Billerica, MA). Low retention 0.02 μm and 0.1 μm Whatman Anotop 10 filters were purchased from GE Healthcare Life Sciences (Pittsburgh, PA).

2.2 Synthesis of block copolypeptides genes

All block copolypeptide genes were synthesized from synthetic oligomers using plasmid reconstruction recursive directional ligation (PRe-RDL).[25] The block copolypeptides have the form G - $(QYPSDGRG)_n$-$(XGVPG)_{80}$-Y where the resilin-like polypeptide (RLP) length n (20, 40, 60, 80, or 100) and the elastin-like polypeptide (ELP) guest residue (A/G, S, V) are systematically varied (Table 1). A guest residue of A/G indicates that the guest residue alternates between A and G from one pentapeptide to the next, resulting in a 50/50 ratio between A and G.

2.3 Expression and purification of block copolypeptides

Each block copolypeptide was expressed in BL21(DE3) E. coli using a previously published hyperexpression protocol, which relies on the leakiness of the T7 promoter.[26] 5 mL cultures were grown overnight and used to inoculate 1 L flasks of TBDry supplemented with 45 μg/mL kanamycin. The flasks were then incubated at 37°C for 24 h and 190 rpm. Each construct was purified using the previously described inverse transition cycling method.[27–28] Briefly, the cell suspension was centrifuged at 3,000 rpm for 10 min at 4°C, the cell pellet resuspended in PBS and then lysed by sonication on ice for 3 min (10 s on, 40 s off) (Masonix S-4000; Farmingdale, NY). Polyethyleneimine (PEI) 0.7% w/v was added to the lysate to precipitate nucleic acid contaminants. The supernatant was then subjected to multiple rounds of ITC as follows: the solution was kept on ice, and 3 M NaCl was added to isothermally trigger the phase transition of the ELP. The coacervate was then centrifuged for 20 min at 14,000 g and 20°C, the supernatant was decanted and discarded, and the pellet was resuspended in phosphate buffer. This suspension was cooled to 4°C, and then centrifuged for 10 min at 14,000 and 4°C to remove any insoluble contaminants. Purity of the block copolypeptides was assessed via SDS-PAGE gel and $CuCl_2$ staining (Figure S2).

2.4 Thermal turbidimetry

Turbidity profiles were obtained for each of the constructs by recording the optical density as a function of temperature (1°C/min ramp) on a temperature controlled UV-Vis spectrophotometer (Cary 300 Bio; Varian Instruments; Palo Alto, CA). The transition temperature (Tt) was defined as the inflection point of the turbidity profile. Samples were measured in PBS at 10 μM. Because some of the block copolypeptides which form larger micelles are slightly turbid when soluble, all measurements were taken after zeroing with PBS.

2.5 Static and dynamic light scattering

Static and dynamic light scattering measurements (SLS/DLS) were performed using an ALV/CGS-3 goniometer system (Langen, Germany). Samples for the ALV/CGS-3 goniometer system were prepared at a concentration of 10 μM in PBS and filtered through 0.45 μm Millex- GV filters into a 10 mm diameter disposable borosilicate glass tube (Fischer). Simultaneous SLS and DLS measurements were obtained at 15 °C of the ELP for angles between 30°−150° at 5° increments, with each angle consisting of 3 runs for 15 s. SLS experiments were only conducted for self-assembling block copolypeptides, since the molecular weight of a single block copolypeptide chain is already known, and the R_g of a single chain is likely near or below the detection limit of the SLS instrument. The differential refractive index (dn/dc) was determined by measuring the refractive index at different concentrations using an Abbemat 500 refractometer (Anton Paar, Graz, Austria). DLS data were analyzed by fitting the autocorrelation function with a cumulant fit, using the built-in ALV software. Hydrodynamic radius (Rh) was plotted against angle and extrapolated to zero. SLS data were analyzed by partial Zimin plots using ALVSTAT software to determine the R_g and molecular weight (MW).

2.6 Temperature-programmed dynamic light scattering

For one sample whose LCST phase transition was not visible via thermal turbidimetry (RLP_{40} - $ELP_{A/G,80}$), temperature-programmed dynamic light scattering was used to identify the transition temperature (T_t). Temperature-programmed dynamic light scattering experiments were carried out using a Dynapro plate reader (Wyatt Technology; Santa Barbara, CA) with samples filtered through 0.45 μm Millex-GV filters. Data was collected at increments of 1 °C, and the cumulant fit hydrodynamic radius was taken as the radius. The T_t was defined as the temperature at which aggregates of size hundreds of nanometers were formed.

2.7 Cryogenic transmission electron microscopy

Cryo-TEM experiments were performed at Duke University's Shared Materials Instrumentation Facility (Durham, NC). Lacey holey carbon grids (Ted Pella, Redding, CA) were glow discharged in a PELCO EasiGlow Cleaning System (Ted Pella, Redding, CA). A 3 μL drop (200 μM ELP concentration) was deposited onto the grid, blotted for 3 s with an offset of −3 mm, and vitrified in liquid ethane using the Vitrobot Mark III (FEI, Eindhoven, Netherlands). Prior to vitrification, the sample chamber was maintained at 15 °C and 100% relative humidity to prevent sample evaporation. Grids were transferred to a Gatan 626 cryoholder (Gatan, Pleasanton, CA) and imaged with an FEI Tecnai G2 Twin TEM (FEI, Eindhoven, Netherlands), operating at 80 keV. Feature sizes and spacing distances were measured in ImageJ by manual measurement of at least 25 distances.[29]

2.8 Small-angle neutron scattering

SANS experiments were conducted at the NIST Center for Neutron Research (NCNR) on the NGB 30m SANS instrument. Samples were poured into quartz cuvettes and acquisitions were performed at 15 °C. All samples were measured in PBS with D2O as a solvent to have good contrast conditions (difference in scattering length densities, ΔSLD) and a lower incoherent background (mainly caused by hydrogen atoms). Three configurations were used with a fixed wavelength of 0.6 nm and sample-detector distances of 1.33 m, 4 m, and 13.17 m corresponding to q ranging from approximately 0.05 nm-1 to 5 nm-1. Data were reduced using the NCNR SANS reduction macros in Igor Pro [30], which allows for the correction of intensities for the transmission, dead-time, detector background (with B4C as a neutron absorber at the sample position), and sample background (either the empty cuvette or the solvent). Absolute intensity was obtained from a tabulated value of a 1.5 mm sheet of Plexiglass.

3. Results and discussion

Recombinant DNA techniques were used to synthesize a family of block copolypeptides in which the RLP length *n* and the ELP guest residue X were systematically varied. (See Supplemental Information for gene sequences.) We refer to the RLP block with the notation RLP_n, where n denotes the number of octapeptide repeats of the sequence QYPSDGRG, and the ELP block with the notation $ELP_{x,80}$ where X denotes the guest residue, and 80 denotes the number of VPGXG pentapeptide repeats in the ELP segment. The first set of five diblock polypeptides consists of polymers in which the ELP block is $ELP_{A/G,80}$ that has an equal

number of Ala (A) and Gly (G) residues at the guest residue position of the ELP, and the RLP length is varied between 20 and 100 octapeptides. This set allows us to determine how the molecular weight of the core-forming RLP block affects self-assembly. The second set consists of RLP_{40} and RLP_{80} fused to $ELP_{S,80}$ and $ELP_{V,80}$, with Ser (S), and Val (V) as the guest residues, respectively, allowing us to investigate the effect of replacing the $ELP_{A/G,80}$ with a more hydrophilic ($ELP_{S,80}$) or more hydrophobic ELP ($ELP_{V,80}$). The third set consists of RLP_{40}-$ELP_{A/G,160}$, RLP_{20}-$ELP_{A/G,40}$, RLP_{80}-$ELP_{A/G;160}$, and RLP_{40}-$ELP_{A/G,40}$, allowing us to investigate the effect of overall chain length, independent of the hydrophilic weight fraction.

The phase behavior of all block copolypeptides with 80 ELP repeats is shown in Figure 1; the turbidity profiles are shown in Figure S3. At the transition temperature (T_t) of the ELP block, the block copolypeptides phase transition into a polypeptide-rich coacervate. The only exception was RLP_{20}-$ELP_{A/G,80}$, which has the most hydrophilic RLP block, and which did not exhibit an LCST phase transition in the observable range (5^{o}C-90^{o}C). No UCST phase transition was observed as the solution temperature was raised above the LCST phase transition for any block copolypeptide. The T_t of the ELP block depends upon its hydrophilicity, with more hydrophilic ELP blocks exhibiting a higher T_t. Interestingly, the RLP block plays a role in modulating the T_t of the ELP block, as fusion to longer RLP blocks lowers the T_t.

A UCST phase transition was only observed for one diblock copolypeptide RLP_{40}-$ELP_{S,80}$, which transitions from micelles to soluble chains at 35 °C before undergoing its LCST phase transition from soluble chains to a coacervate at 58 °C (Fig. S2e). The absorbance of a second block copolypeptide - RLP_{100}-$ELP_{A/G,80}$ - also decreases before increasing at its LCST phase transition (Figure S3b). However, unlike RLP_{40}-$ELP_{S,80}$, RLP_{100}-$ELP_{A/G,80}$ is turbid even when soluble because it forms large micelles at low temperatures (Table 2). Thus, unlike RLP40- $ELP_{S,80}$, the turbidity decreases but the solution still remains turbid, indicating that there is not a UCST phase transition and the micelles do not disassemble.

All block copolypeptides were next characterized by static and dynamic light scattering (SLS/DLS) at 15 °C, to determine the number of polymer chains (N_{agg}) per nanostructure, and the radius of gyration (R_g) and hydrodynamic radius (R_h) of the nanostructures (Table 2). The shape factor $\rho = R_g/R_h$ gives an indication of the morphology, with 1.505 corresponding to a Gaussian polymer chain, 1.0 to a hollow sphere or vesicle, and 0.775 to a solid sphere. For an elongated scatterer, the shape factor depends upon the aspect ratio. [31]

Within the first set of RLP-ELPs wherein we systematically varied the length of the RLP block from 20 to 100 pentapeptides, while keeping the composition and length of the ELP block constant, the light scattering data reveal three distinct behaviors of self-assembly. First, RLP_{20} – $ELP_{A/G,80}$ is fully soluble and does not self-assemble. Second, RLP_{40}-$ELP_{A/G,80}$ and RLP_{60}- $ELP_{A/G,80}$ self-assemble into structures with R_h of 30–40 nm, $\rho < 1$, and low N_{agg}, indicating that both diblocks likely self-assemble into spherical micelles. Third, RLP_{80}-$ELP_{A/G,80}$ and RLP_{100}- $ELP_{A/G,80}$ self-assemble into much larger structures with characteristic ratios above 1 and high aggregation numbers, indicating that they likely self-assemble into much larger, non-spherical structures. These results clearly show that

increasing the length of a RLP block while holding the composition and length of the ELP block is enough to modulate self-assembly, indicating that *the RLP block length is a unique molecular parameter to independently tune self-assembly of these diblock copolymers.*

In the second set, we varied the hydrophilicity of the corona-forming elastin-like polypeptide (ELP) block, to investigate the effect of corona chain hydrophilicity on self-assembly. To do so, the ELP block length was held constant at 80 pentapeptides, but the composition was varied from S (hydrophilic) to V (hydrophobic) guest residues, to investigate the impact of the hydrophobicity of the ELP block on self-assembly. In this series, the ELP length was also toggled between 40 and 80 pentapeptides to examine how the RLP block length affects self-assembly. Equivalent length block copolypeptides — RLP_{40}-$ELP_{A/G,80}$ and RLP_{80}-$ELP_{A/G,80}$ — from the first set are also included in the analysis of this set, as their A and G guest residues have a hydrophobicity that is intermediate between S and V. Comparison of these three sets by varying hydrophobicity shows that when $ELP_{A/G,80}$ is replaced by the more hydrophilic $ELP_{S,80}$, the light scattering results indicate that the spherical morphology of $ELP_{A/G,80}$ is unaffected. However, when $ELP_{A/G,80}$ is replaced by the more hydrophobic $ELP_{V,80}$, larger, non-spherical structures are formed, as suggested by the p of 1.00, indicating that the morphology is affected above a threshold hydrophobicity of the ELP block. The trends in morphology for the RLP_{40}- ELP_{80} copolypeptides in this set are consistent with this notion, as an increase in hydrophobicity from S to A/G in this series appear to have no impact on the spherical morphology, as the p remains close to 0.8, but the increase in ρ to 1.04 for the RLP_{40} - $ELP_{V,80}$ is suggestive of a switch to a more elongated rod-like morphology. The most important observation from this set is that *increasing the hydrophobicity of the corona-forming ELP decreases the repulsion between corona chains, causing a transition from spherical to cylindrical morphology.*

The third set contains RLP-ELPs that when analyzed with corresponding RLP-ELPs from sets 1 and 2 allowed us to examine the effect of molecular weight on self-assembly, while keeping the hydrophilic weight fraction constant. In this set, RLP_{40}-$ELP_{A/G,160}$ self-assembled into spherical micelles, as suggested by its shape factor of approximately 0.5. This demonstrates that the hydrophilic weight fraction alone is not a sufficient condition for self-assembly, as RLP_{20}- $ELP_{A/G,80}$ from set 1, despite having the same hydrophilic weight fraction as RLP_{40}-$ELP_{A/G,160}$, did not self-assemble (Table 2, R_h = 5.4 nm). Consistent with this observation, RLP_{20}-$ELP_{A/G,40}$ also did not self-assemble while RLP_{80}-$ELP_{A/G,160}$, which has the same hydrophilic weight fraction, in contrast, self-assembles into spherical micelles (Table 2, shape factor = 0.84). The lack of self-assembly of the two RLP-ELPs with the shortest, 20 octapeptide blocks, is driven by the short length of the RLP block, suggesting that *independent of the length of the corona forming ELP block there is a minimum threshold in the length of the RLP block, below which self-assembly does not occur.* The formation of a spherical morphology is driven by the hydrophilic weight fraction: both RLP_{40}-$ELP_{A/G,80}$ (from Set 1) and RLP_{80} – $ELP_{A/G,160}$ self- assemble into spherical micelles. The micelles formed by RLP_{80}-$ELP_{A/G,160}$ are larger than those formed by RLP_{40}-$ELP_{A/G,80}$ that have the same hydrophilic: hydrophobic ratio, consistent with the higher molecular weight. Finally, RLP_{40}-$ELP_{A/G,40}$ has a characteristic ratio well above 1, indicating likely self-assembly into cylindrical micelles, consistent with RLP_{80}-$ELP_{A/G,80}$ (from set 1) which has the same hydrophilic weight fraction.

To further characterize the morphology of the self-assembled structures, all self-assembling block copolypeptides were characterized by cryo-TEM (Figures 2–4). In the first set (Figure 2), RLP_{40}-$ELP_{A/G,80}$ (Figure 2A) and RLP_{60}-$ELP_{A/G,80}$ (Figure 2B) both self-assemble into spherical micelles. Measurements of the core radii indicate that RLP_{40}-$ELP_{A/G,80}$ and RLP_{60}-$ELP_{A/G,80}$ cores are approximately 12.8 nm and 17.5 nm, consistent with a larger core-forming block leading to a larger micelle core (Table S2). RLP_{40}-$ELP_{A/G,80}$ also appears to form a few elongated, cylindrical micelles in the center of the film, where the ice layer is the thinnest. It is not clear from cryo-TEM whether this morphology exists normally in the dilute solution conditions that the light scattering was carried out in, or if it is an artifact of the sample preparation process, which concentrates the block copolypeptide into a thin vitreous ice layer and selectively partitions it to the center of the film. Both light scattering (Table 2) and small-angle neutron scattering (below, Figure 5) help resolve this question.

Cryo-TEM reveals that RLP_{80}-$ELP_{A/G,80}$ (Figure 2C) and RLP_{100}-$ELP_{A/G,80}$ (Figure 2D) form an entirely different nanostructure. Both block copolypeptides form long, overlapping cylindrical structures, with some spherical structures visible as well. Because these experiments were conducted at 10 μM, which is well below the overlap concentration, these cryo-TEM data indicate that during the vitrification process, these block copolypeptides preferentially partition into the thin vitreous ice layer, leading to a higher concentration than is observed in solution. Thus, it is unclear from cryo-TEM alone whether these block copolypeptides truly form micellar structures in dilute solution. Light scattering (Table 2) and small-angle neutron scattering (below, Figure 3) experiments were hence conducted to resolve this question.

Analyzing the cryo-TEM data, we find that the spacing between micelle cores increased considerably from 47.7 nm for RLP_{80}-$ELP_{A/G,80}$ to 70.1 nm for RLP_{i00}-$ELP_{A/G80}$ (Table S2). This is consistent with geometric arguments from polymer physics: as the cylindrical micelles increase in size and incorporate more polypeptide chains, the density of chains increases (consistent with light scattering, Table 2), leading to increased repulsion between corona chains, a more extended ELP chain conformation, and increased spacing of RLP_{100}-$ELP_{A/G80}$ relative to RLP80-$ELP_{A/G,80}$.

Cryo-TEM results for the second set (Figure 3) indicate that when $ELP_{A/G,80}$ is replaced by the more hydrophilic $ELP_{S,80}$, spherical micelles are formed for both RLP block lengths — RLP_{40}-$ELP_{S,80}$, (Figure 3A) and RLP_{80}-$ELP_{S,80}$ (Figure 3B). In contrast, when $ELP_{A/G,80}$ is replaced by the more hydrophobic $ELP_{V,80}$, cylindrical micelles are formed with both RLP blocks — RLP_{40}-$ELP_{V,80}$, (Figure 3C) and RLP_{80}-$ELP_{V,80}$, (Figure 3D).

In the third set (Figure 4), RLP_{40}-$ELP_{A/G,160}$ and RLP_{80}-$ELP_{A/G,160}$ both self-assemble into spherical micelles (Figure 4A and 4B), with RLP_{80}-$ELP_{A/G,160}$ having a larger micelle core than RLP_{40}-$ELP_{A/G,160}$ (33.0 nm vs 12.0 nm, Table S2). RLP_{40}-$ELP_{A/G,40}$ forms cylindrical micelles (Figure 4C) with cores smaller than those of RLP_{80} - $ELP_{A/G,80}$ (13.2 nm vs 27.7 nm, Table S2).

To better understand the morphology of the self-assembled micelles, and specifically to determine whether the overlapping cylindrical micelle structures observed in Figure 2 truly occur in dilute solution, RLP_{40}-$ELP_{A/G,80}$ and RLP_{80}-$ELP_{A/G,80}$ were characterized by small-angle neutron scattering (SANS). These diblock polypeptides were selected because they represent the two main morphologies observed by light scattering and cryo-TEM. A SANS spectrum for each diblock polypeptide is shown in Figure 5.

Even in the absence of a model-dependent analysis, one can observe visually that RLP_{80}-$ELP_{A/G,80}$ has a larger size (due to its kink at a lower q of ~ 0.15 nm^{-1}) and a larger aggregation number due to its higher forward scattering value than RLP_{40}-$ELP_{A/G,80}$ (30.9 cm^{-1} vs. 5.9 cm^{-1}). Additionally, the RLP_{80}-$ELP_{A/G,80}$ curve continues to increase at low q, indicating that the long dimension of these micelles is beyond the range observable by SANS. To obtain a more complete picture of the self-assembly of these diblock polypeptides, we then fit their SANS spectra using analytical shape models (Figure 5, Supporting Information Table S3). The data were best fit by the spherical (RLP_{40}-$ELP_{A/G,80}$) and cylindrical (RLP_{80}-$ELP_{A/G,80}$) block copolymer micelle form factors developed by Gerstenberg and Pedersen. [32] (Full model details are provided in the Supporting Information.) The fit parameters (Table 3) are in good agreement with both the light scattering data (Table 2) and cryo-TEM images (Figures 2–4). (The model does not fit the data well at high q for RLP_{80} - $ELP_{A/G,80}$ because the data is highly sensitive to the subtraction of the incoherent background.)

The self-assembly behavior of the RLP-ELP diblock polypeptides as a function of structural parameters are summarized in Figure 6. For a hydrophilic block of $ELP_{A/G,80}$, increasing the size of hydrophobic block from RLP_{20} to RLP_{40} leads to increased interactions between the hydrophobic blocks and a transition from fully soluble unimers to self-assembly into spherical micelles (Figure 6A, 1). With the same $ELP_{A/G,80}$ hydrophilic block, further increasing the size of the hydrophobic block from RLP_{60} to RLP_{80} leads to a transition from spherical to cylindrical micelles (Figure 6A, 2). With a hydrophobic block of RLP_{80}, substituting the more hydrophilic $ELP_{S,80}$ for $ELP_{A/G,80}$ leads to increased repulsion between corona blocks and a transition from a cylindrical to spherical morphology (Figure 6A, 3). Conversely, substituting a more hydrophobic $ELP_{V,80}$ for $ELP_{A/G,80}$ decreases repulsion within the corona chains and leads to a transition from a spherical to cylindrical morphology (Figure 6A, 4). With $ELP_{A/G,80}$, further increasing the size of the hydrophobic block from RLP_{80} to RLP_{100} enhances the tendency towards a cylindrical morphology even further and leads to longer cylinders with a larger aggregation number.

The self-assembly trends remain consistent when the overall chain length is varied. Similar to RLP_{20}-$ELP_{A/G,80}$, RLP_{20}-$ELP_{A/G,40}$ does not self-assemble because RLP_{20} remains fully soluble (Figure 6B, 5). RLP_{40}-$ELP_{A/G,160}$ and RLP_{80}-$ELP_{A/G,160}$ (Figure 6B, 6 and 7) both self-assemble into spherical micelles because of their high hydrophilic weight fractions, similar to RLP_{40} - $ELP_{A/G,80}$. RLP_{40}-$ELP_{A/G,40}$ (Figure 4B, 8) self-assembles into cylindrical micelles because of its lower hydrophilic weight fraction, similar to RLP_{80}-$ELP_{A/G,80}$.

Unlike purely ELP based block copolymers, whose behavior does not obey the canonical principles of self-assembly for diblock polymers predicted by polymer physics, [33] the selfassembly of ELP-RLP diblock copolymers can be understood by simple principles of polymer physics that relate the hydrophilic weight fraction, polymer-polymer and polymer-solvent interactions to micellar morphology. Specifically, the major findings of this study are that: (1) independent of the length of the corona forming ELP block there is a minimum threshold in the length of the RLP block below which self-assembly does not occur, but that once that threshold is crossed, (2) the RLP block length is a unique molecular parameter to independently tune self-assembly; and (3) increasing the hydrophobicity of the corona forming ELP drives a transition from spherical to cylindrical morphology. These results are unique because they are the first instance of a recombinant diblock polypeptide system whose self-assembly is so clearly governed by simple principles from polymer physics. These findings are also important because they provide a rational approach for the de novo design of desired nanoscale morphologies from first principles, that we believe will lead to biomedical applications, such as the design of nanoscale drug delivery vehicles. [34] We anticipate exploring these applications in future studies.

Supplementary Material

Refer to Web version on PubMed Central for supplementary material.

ACKNOWLEDGMENT

This work was supported by the NIH through grant R01 GM-61232 to A.C. and by the Research Triangle MRSEC (DMR-11–21107). We acknowledge the support of the National Institute of Standards and Technology, U.S. Department of Commerce, in providing the neutron research facilities used in this work. We acknowledge the Duke University Shared Materials and Instrumentation Facility for maintaining the cryo-TEM instrument used in this work. I.W. would like to thank the International Graduate Research Training Group 1524 (IGRTG) and the Department of Physical Chemistry at T.U. Berlin for graciously hosting him in 2013 and 2015.

Funding Sources

This work was supported by the NSF through the Research Triangle MRSEC (DMR-11–21107), the NIH through grant R01-GM61232 to A.C., and by the Bundesministerium für Bildung und Forschung (BMBF) Project No. 05K13KT1. I.W. acknowledges support in the form of a National Science Foundation Graduate Research Fellowship (DGE-1106401). This work utilized facilities supported in part by the National Science Foundation under Agreement No. DMR-0944772.

REFERENCES

1. Mai Y; Eisenberg A, Self-assembly of block copolymers. Chem. Soc. Rev. 2012, 41 (18), 5969–5985. [PubMed: 22776960]
2. Letchford K; Burt H, A review of the formation and classification of amphiphilic block copolymer nanoparticulate structures: micelles, nanospheres, nanocapsules and polymersomes. European journal ofpharmaceutics and biopharmaceutics 2007, 65 (3), 259–269.
3. Gaucher G; Dufresne M-H; Sant VP; Kang N; Maysinger D; Leroux J-C, Block copolymer micelles: preparation, characterization and application in drug delivery. J. Controlled Release 2005, 109 (1–3), 169–188.
4. Discher BM; Won Y-Y; Ege DS; Lee JC; Bates FS; Discher DE; Hammer DA, Polymersomes: tough vesicles made from diblock copolymers. Science 1999, 284 (5417), 1143–1146. [PubMed: 10325219]

5. Bassett DC; Frank FC; Keller A, Lamellae and their Organization in Melt- Crystallized Polymers [and Discussion]. Philosophical Transactions of the Royal Society of London. Series A : Physical and Engineering Sciences 1994, 348 (1686), 29–43.
6. Allen G; Baker C, Lower critical solution phenomena in polymer-solvent systems. Polymer 1965, 6 (4), 181–191.
7. Gandhi A; Paul A; Sen SO; Sen KK, Studies on thermoresponsive polymers: Phase behaviour, drug delivery and biomedical applications. asian journal of pharmaceutical sciences 2015, 10 (2), 99–107.
8. Virtanen J; Arotcarena M; Heise B; Ishaya S; Laschewsky A; Tenhu H, Dissolution and aggregation of a poly (NIPA-block-sulfobetaine) copolymer in water and saline aqueous solutions. Langmuir 2002, 18 (14), 5360–5365.
9. Maeda Y; Mochiduki H; Ikeda I, Hydration changes during thermosensitive association of a block copolymer consisting of LCST and UCST blocks. Macromol. Rapid Commun. 2004, 25 (14), 1330–1334.
10. Shih Y-J; Chang Y; Deratani A; Quemener D, “Schizophrenic” hemocompatible copolymers via switchable thermoresponsive transition of nonionic/zwitterionic block self-assembly in human blood. Biomacromolecules 2012, 13 (9), 2849–2858. [PubMed: 22838402]
11. Arotcarena M; Heise B; Ishaya S; Laschewsky A, Switching the inside and the outside of aggregates of water-soluble block copolymers with double thermoresponsivity. J. Am. Chem. Soc. 2002, 124 (14), 3787–3793. [PubMed: 11929270]
12. Weaver J; Armes S; Butun V, Synthesis and aqueous solution properties of a well- defined thermo-responsive schizophrenic diblock copolymer. Chem. Commun. (Cambridge, U. K.) 2002, (18), 2122–2123.
13. Jun YJ; Toti US; Kim HY; Yu JY; Jeong B; Jun MJ; Sohn YS, Thermoresponsive Micelles from Oligopeptide □ Grafted Cyclotriphosphazenes. Angewandte Chemie International Edition 2006, 45 (37), 6173–6176. [PubMed: 16906609]
14. Yuan W; Zou H; Guo W; Wang A; Ren J, Supramolecular amphiphilic star- branched copolymer: from LCST-UCST transition to temperature-fluorescence responses. J. Mater. Chem. 2012, 22 (47), 24783–24791.
15. Quiroz FG; Chilkoti A, Sequence heuristics to encode phase behaviour in intrinsically disordered protein polymers. Nat. Mater. 2015, 14 (11), 1164–71. [PubMed: 26390327]
16. Elvin CM; Carr AG; Huson MG; Maxwell JM; Pearson RD; Vuocolo T; Liyou NE; Wong DC; Merritt DJ; Dixon NE, Synthesis and properties of crosslinked recombinant pro-resilin. Nature 2005, 437 (7061), 999–1002. [PubMed: 16222249]
17. Nairn KM; Lyons RE; Mulder RJ; Mudie ST; Cookson DJ; Lesieur E; Kim M; Lau D; Scholes FH; Elvin CM, A synthetic resilin is largely unstructured. Biophys. J. 2008, 95 (7), 3358–3365. [PubMed: 18586853]
18. Lyons RE; Lesieur E; Kim M; Wong DC; Huson MG; Nairn KM; Brownlee AG; Pearson RD; Elvin CM, Design and facile production of recombinant resilin-like polypeptides: gene construction and a rapid protein purification method. Protein Engineering Design and Selection 2007, 20 (1), 25–32.
19. Hassouneh W; Fischer K; MacEwan SR; Branscheid R; Fu CL; Liu R; Schmidt M; Chilkoti A, Unexpected multivalent display of proteins by temperature triggered self-assembly of elastin-like polypeptide block copolymers. Biomacromolecules 2012, 13 (5), 1598–605. [PubMed: 22515311]
20. Dreher MR; Simnick AJ; Fischer K; Smith RJ; Patel A; Schmidt M; Chilkoti A, Temperature Triggered Self-Assembly of Polypeptides into Multivalent Spherical Micelles. J. Am. Chem. Soc. 2007, 130 (2), 687–694. [PubMed: 18085778]
21. McDaniel JR; Weitzhandler I; Prevost S; Vargo KB; Appavou M-S; Hammer DA; Gradzielski M; Chilkoti A, Noncanonical Self-Assembly of Highly Asymmetric Genetically Encoded Polypeptide Amphiphiles into Cylindrical Micelles. Nano Lett. 2014, 14 (11), 6590–6598. [PubMed: 25268037]
22. Zhang L; Eisenberg A, Multiple morphologies of” crew-cut” aggregates of polystyrene-b-poly (acrylic acid) block copolymers. Science 1995, 268 (5218), 1728. [PubMed: 17834990]

23. Discher DE; Eisenberg A, Polymer vesicles. Science 2002, 297 (5583), 967–973. [PubMed: 12169723]
24. Srinivas G; Discher DE; Klein ML, Self-assembly and properties of diblock copolymers by coarse-grain molecular dynamics. Nat. Mater. 2004, 3 (9), 638–44. [PubMed: 15300242]
25. McDaniel JR; Mackay JA; Quiroz FG; Chilkoti A, Recursive directional ligation by plasmid reconstruction allows rapid and seamless cloning of oligomeric genes. Biomacromolecules 2010, 11 (4), 944–52. [PubMed: 20184309]
26. Guda C; Zhang X; Mcpherson DT; Xu J; Cherry JH; Urry DW; Daniell H, Hyper Expression of an Environmentally Friendly Synthetic-Polymer Gene. Biotechnol. Lett. 1995, 17 (7), 745–750.
27. Meyer DE; Chilkoti A, Purification of recombinant proteins by fusion with thermally- responsive polypeptides. Nat. Biotechnol. 1999, 17 (11), 1112–5. [PubMed: 10545920]
28. Trabbic-Carlson K; Liu L; Kim B; Chilkoti A, Expression and purification of recombinant proteins from Escherichia coli: Comparison of an elastin-like polypeptide fusion with an oligohistidine fusion. Protein Sci. 2004, 13 (12), 3274–84. [PubMed: 15557268]
29. Schneider CA; Rasband WS; Eliceiri KW, NIH Image to ImageJ: 25 years of image analysis. NatMeth 2012, 9 (7), 671–675.
30. Kline S, Reduction and analysis of SANS and USANS data using IGOR Pro. J. Appl. Crystallogr. 2006, 39 (6), 895–900.
31. Ortega A; García de la Torre J, Hydrodynamic properties of rodlike and disklike particles in dilute solution. The Journal of Chemical Physics 2003, 119 (18), 9914–9919.
32. Pedersen JS; Gerstenberg MC, Scattering Form Factor of Block Copolymer Micelles. Macromolecules 1996, 29 (4), 1363–1365.
33. Garanger E; MacEwan SR; Sandre O; Brulet A; Bataille L; Chilkoti A; Lecommandoux S, Structural Evolution of a Stimulus-Responsive Diblock Polypeptide Micelle by Temperature Tunable Compaction of its Core. Macromolecules 2015, 48 (18), 6617–6627.
34. Geng Y; Dalhaimer P; Cai S; Tsai R; Tewari M; Minko T; Discher DE, Shape effects of filaments versus spherical particles in flow and drug delivery. Nat. Nanotechnol. 2007, 2(4), 249–55. [PubMed: 18654271]

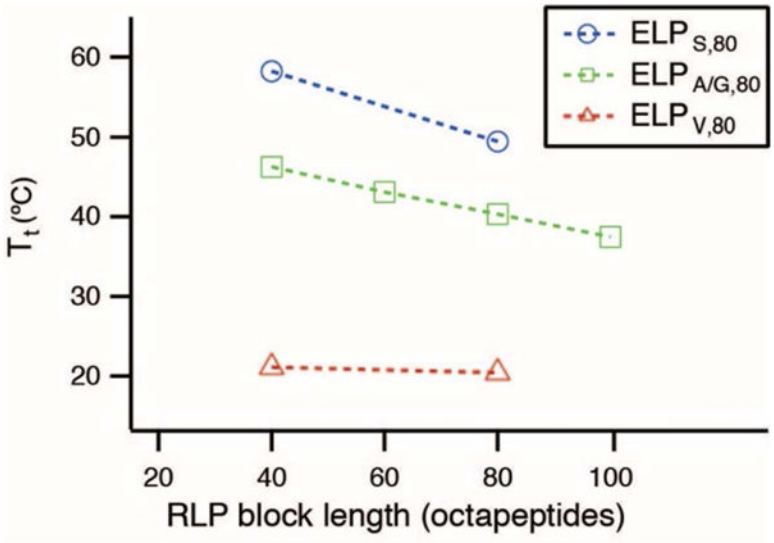

Figure 1.

LCST phase behavior of block copolypeptides. (RLP_{40} - $ELP_{S,80}$ undergoes a UCST phase transition from micelles to soluble chains at 35 °C before undergoing its LCST at 58 °C.)

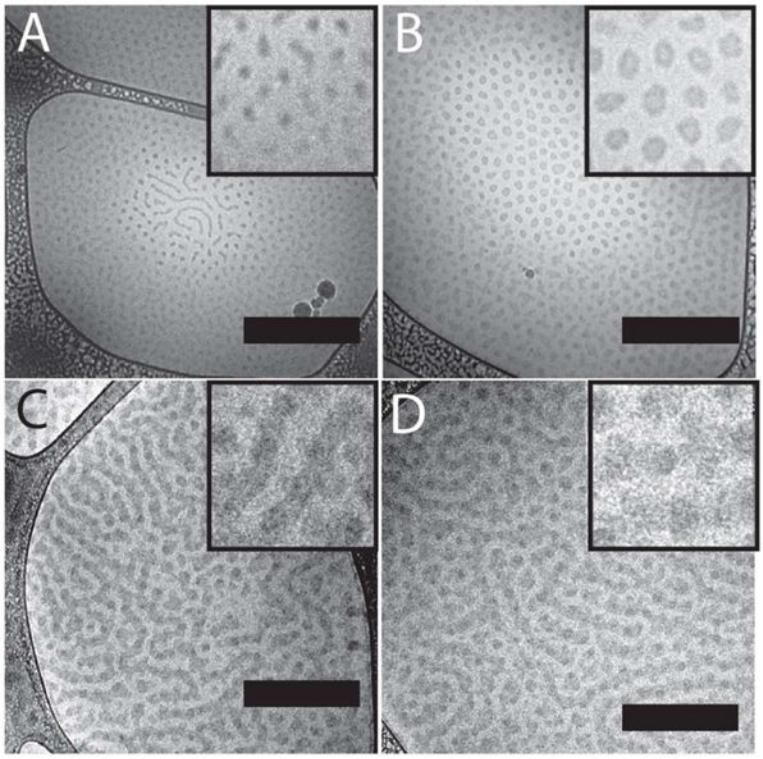

Figure 2.

Cryo-TEM micrographs of RLP-ELPs in set 1 (a, b) spherical micelles formed by RLP_{40}-$ELP_{A/G,80}$ and RLP_{60}-$ELP_{A/G,80}$, (c,d) cylindrical micelles formed by RLP_{80}-$ELP_{A/G,80}$, RLP_{100}-$ELP_{A/G,80}$. Scale bars 500 nm. All insets 250 nm by 250 nm. (Additional micrographs in Figures S14 - S17).

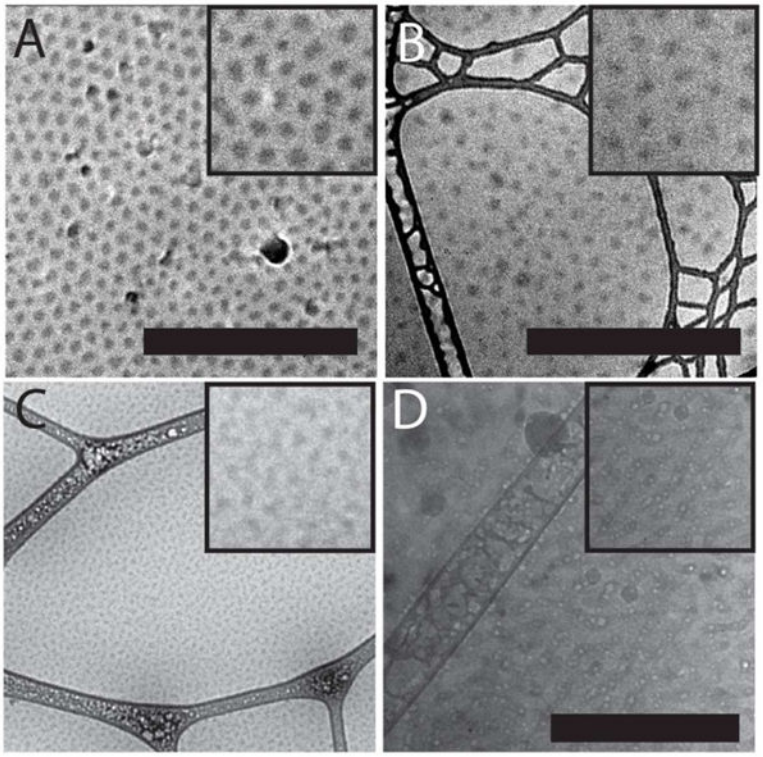

Figure 3.

Cryo-TEM micrographs of RLP-ELPs in set 2: (a,b,c) spherical micelles formed by RLP_{40} – $ELP_{S,80}$, RLP_{80} – $ELP_{S,80}$, and RLP_{40} – $ELP_{V,80}$, (d) cylindrical micelles formed by RLP_{80} – $ELP_{V,80}$. Scale bars 500 nm (a-c), 200 nm (d). All insets 250 nm by 250 nm. (Additional micrographs in Figures S18 - S21).

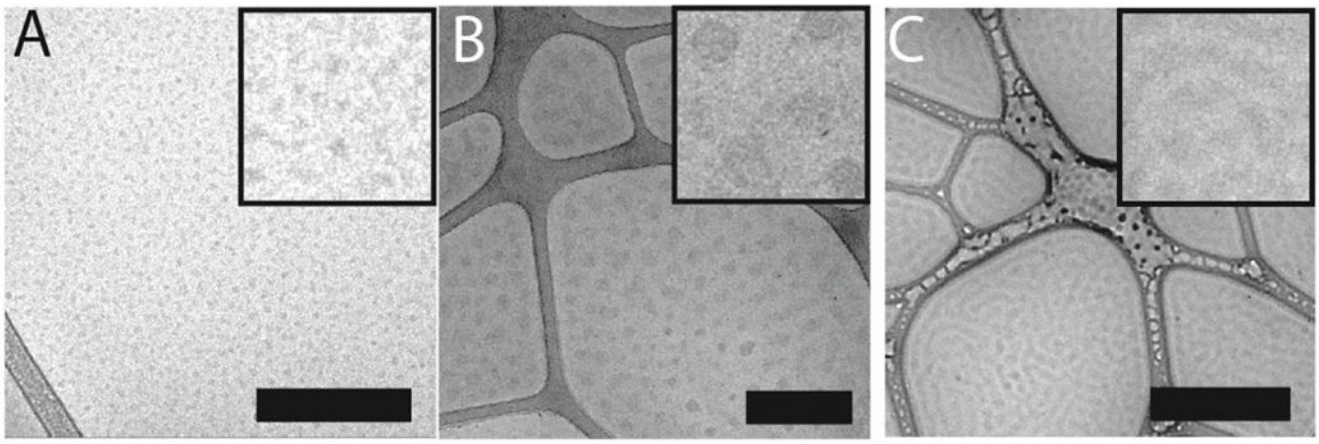

Figure 4.

Cryo-TEM micrographs of RLP-ELPs in set 3: (a) spherical micelles formed by RLP_{40}-$ELP_{A/G,160}$, (b) spherical micelles formed by RLP_{80}-$ELP_{A/G,160}$, and (c) cylindrical micelles formed by RLP_{40}-$ELP_{A/G,40}$. Scale bars 500 nm. All insets 250 nm by 250 nm. (Additional micrographs in Figures S14 - S24).

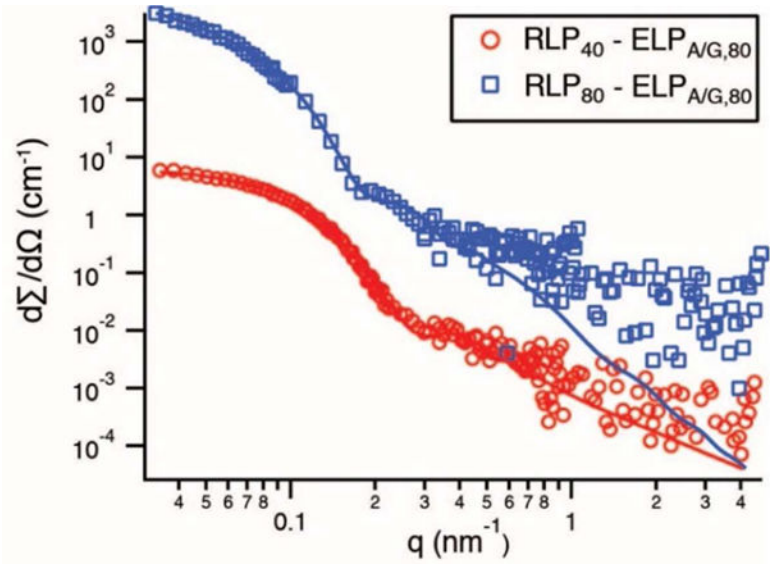

Figure 5.

SANS spectra and analytical model fits for RLP_{40}-$ELP_{A/G,80}$ and (C) RLP_{80}-$ELP_{A/G,80}$. (The spectrum for RLP_{80}-$ELP_{A/G,80}$ is offset by a factor of 100 for clarity.) (Analytical model details in SI).

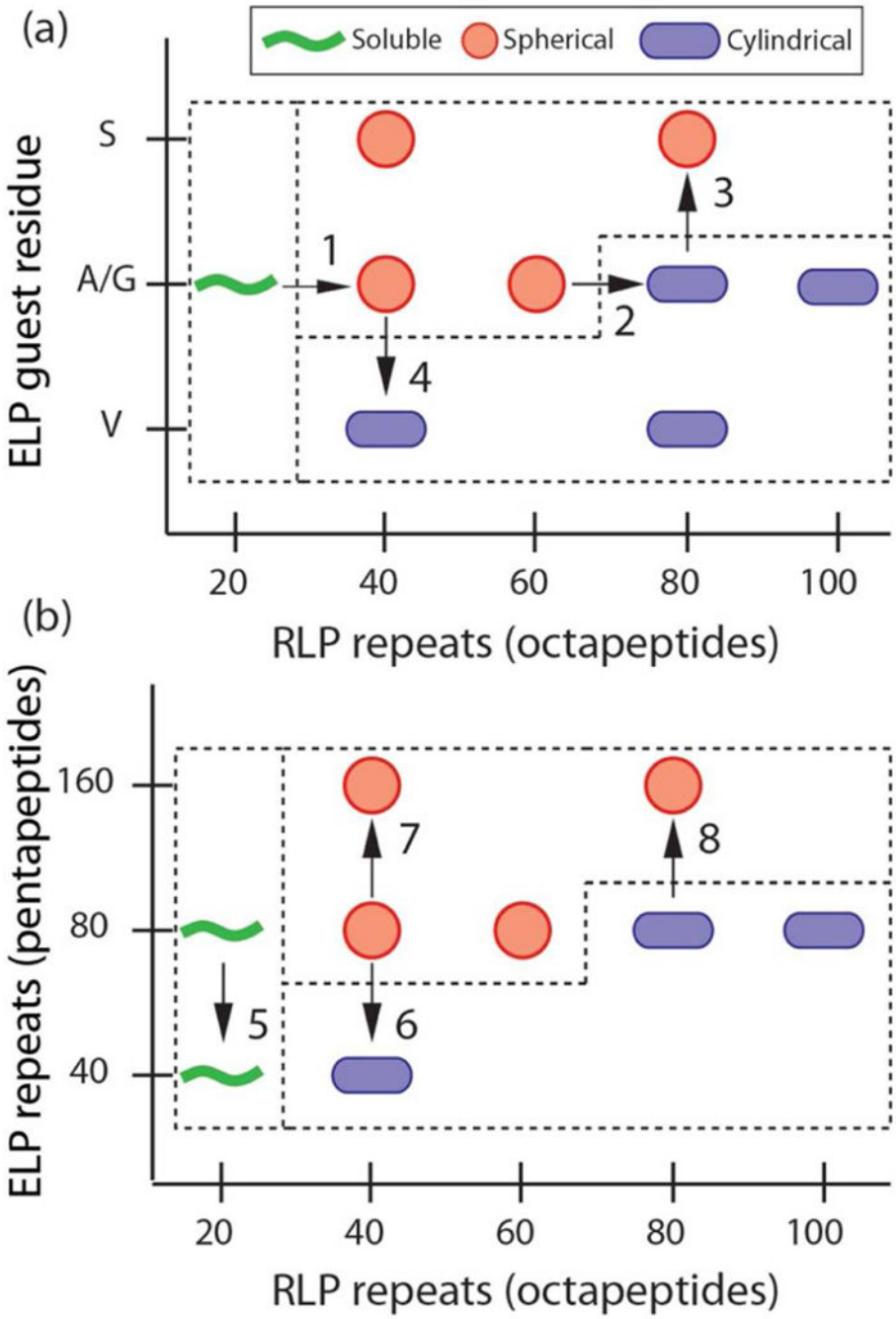

Figure 6.

Quasi-phase diagrams illustrating trends in RLP-ELP self-assembly. (a) Trends in set 1 and set 2, block copolypeptides with the motif $ELP_{Y,80}$-RLP_x. ELP hydrophilicity increases from ELP_V to $ELP_{A/G}$ and ELP_S. (b) Trends in set 1 and set 3, block copolypeptides with the motif $ELP_{A/G,Y}$-RLP_X.

Table 1.

Block copolypeptide nomenclature, sequences, molecular weights, and hydrophilic weight percentages.

	Block copolypeptides	Sequence	MW (kDa)	Hphilic wt%
Set 1	RLP_{20} — $ELP_{A/G,80}$	G-$(QYPSDGRG)_{20}$- $[(A/G)GVPG]_{80}$-Y	47.79	0.63
	RLP_{40} — $ELP_{A/G,80}$	G-$(QYPSDGRG)_{40}$- $[(A/G)GVPG]_{80}$-Y	65.01	0.46
	RLP_{60} — $ELP_{A/G,80}$	G-$(QYPSDGRG)_{60}$- $[(A/G)GVPG]_{80}$-Y	82.24	0.37
	RLP_{80} — $ELP_{A/G,80}$	G-$(QYPSDGRG)_{80}$- $[(A/G)GVPG]_{80}$-Y	99.46	0.30
	RLP_{100} — $ELP_{A/G,80}$	G-$(QYPSDGRG)_{100}$- $[(A/G)GVPG]_{80}$-Y	116.68	0.26
Set 2	RLP_{40} — $ELP_{S,80}$	G-$(QYPSDGRG)_{40}$- $[SGVPG]_{80}$-Y	66.85	0.49
	RLP_{80} — $ELP_{S,80}$	G-$(QYPSDGRG)_{80}$- $[SGVPG]_{80}$-Y	101.30	0.32
	RLP_{40} — $ELP_{V,80}$	G-$(QYPSDGRG)_{40}$- $[VGVPG]_{80}$-Y	67.82	0.50
	RLP_{80} — $ELP_{V,80}$	G-$(QYPSDGRG)_{80}$- $[VGVPG]_{80}$-Y	102.27	0.33
Set 3	RLP_{40} — $ELP_{A/G,160}$	G-$(QYPSDGRG)_{40}$- $[(A/G)GVPG]_{160}$-Y	94.98	0.63
	RLP_{20} — $ELP_{A/G,40}$	G-$(QYPSDGRG)_{20}$- $[(A/G)GVPG]_{40}$-Y	32.41	0.46
	RLP_{80} — $ELP_{A/G,160}$	G-$(QYPSDGRG)_{80}$- $[(A/G)GVPG]_{160}$-Y	129.08	0.46
	RLP_{40} — $ELP_{A/G,40}$	G-$(QYPSDGRG)_{40}$- $[(A/G)GVPG]_{40}$-Y	49.65	0.30

Table 2.

Static and dynamic light scattering characterization of block copolypeptides. Aggregation number N_{agg}, radius of gyration R_g, hydrodynamic radius R_h and the shape factor $\rho = R_g/R_h$ as derived from the light scattering experiments. (Full light scattering data in Figures S4 - S14 and Table S1.)

	Block copolypeptide	**N_{agg}**	**R_g(nm)**	**R_h(nm)**	**$\rho = R_g/R_h$**
Set 1	RLP_{20}—$ELP_{A/G,80}$	-	-	5.5	-
	RLP_{40}—$ELP_{A/G,80}$	68 ± 0.3	29.9 ± 0.6	33.3	0.89
	RLP_{60}—$ELP_{A/G,80}$	231 ± 0.7	23.8 ± 0.5	36.7	0.65
	RLP_{80}—$ELP_{A/G,80}$	2240 ± 84	145.4 ± 5.8	114.3	1.27
	RLP_{100}—$ELP_{A/G,80}$	4463 ±128	187.2 ± 2.5	139.0	1.35
Set 2	RLP_{40}—$ELP_{S,80}$	80 ± 0.5	27.2 ± 0.8	33.0	0.82
	RLP_{80}—$ELP_{S,80}$	392 ± 5.3	36.0 ± 1.4	49.4	0.73
	RLP_{40}—$ELP_{V,80}$	213 ± 0.5	33.1 ± 0.3	31.7	1.04
	RLP_{80}—$ELP_{V,80}$	1329±72	177.3 ± 4.9	176.8	1.00
Set 3	RLP_{40}—$ELP_{A/G,160}$	96 ± 0.4	17.1 ± 0.8	33.8	0.51
	RLP_{20}—$ELP_{A/G,40}$	-	-	5.4	-
	RLP_{80}—$ELP_{A/G,160}$	780 ± 18	65.9 ± 1.5	125.2	0.53
	RLP_{40}—$ELP_{A/G,40}$	83 ± 1.3	42.9 ± 1.3	31.6	1.36

Table 3.

SANS analytical model fit parameters. [a] Rg of corona-forming ELP chains. [b] Volume fraction of water in the micelle core.

Block copolypeptide	Model	R_{core} (nm)	L_{core} (nm)	$R_{g,corona}$ (nm) [a]	$\phi_{H2O,core}$ [b]
RLP_{40} — $ELP_{A/G,80}$	spherical	16.0	N/A	6.3	0.67
RLP_{80} — $ELP_{A/G,80}$	cylindrical	20.2	>250	6.0	0.73